

Magnetoelectric coupling and multi-blocking effect in Ising-chain magnet $\text{Sr}_2\text{Ca}_2\text{CoMn}_2\text{O}_9$

Tathamay Basu,[@] Nahed Sakly, Alain Pautrat, Fabien Veillon, Olivier Pérez, Vincent Caignaert, Bernard Raveau and Vincent Hardy.

CRISMAT, Normandie Univ, ENSICAEN, UNICAEN, CNRS, CRISMAT, 14000 Caen, France.

[@]Present Address : School of Physics and Astronomy, University of Minnesota, Minneapolis, MN, 55455, USA

Abstract

We have demonstrated magnetoelectric (ME) coupling in an Ising-chain magnet $\text{Sr}_2\text{Ca}_2\text{CoMn}_2\text{O}_9$, via detailed investigation of ac susceptibility and dielectric constant as a function of temperature, magnetic field and frequency. $\text{Sr}_2\text{Ca}_2\text{CoMn}_2\text{O}_9$ consists of spin-chains of one CoO_6 trigonal prismatic and two alternating MnO_6 octahedra polyhedron. The $(\text{Co}^{2+} \text{Mn}^{4+} \text{Mn}^{4+})$ distribution stabilizes a $(\uparrow\downarrow\uparrow)$ spin-state along the chains which are distributed on a triangular lattice. This compound undergoes a partially disordered antiferromagnetic transition at $T_N \sim 28$ K. The dielectric constant exhibits a clear peak at T_N only in presence of an external magnetic field ($H \geq 5$ kOe), evidencing the presence of ME coupling, which is further confirmed by H-dependence dielectric measurements. The mechanism of this ME coupling is discussed as a result of exchange-striction in an Ising-chain magnet. In addition to this strong spin-lattice coupling, we report a dipolar relaxation phenomenon similar to spin-relaxation arising from the single-ion magnetism (spin-blocking effect). We term such phenomenon a ‘multi-blocking’ effect.

I. Introduction

Multiferroic and magnetoelectric (ME) materials have been shown to be potential systems for future device application. Various fascinating ME phenomena have been observed in several classes of materials and different mechanisms have been reported that are responsible for the cross-coupling between spins and dipoles. Initially, it was shown that magnetism induced ferroelectricity can be obtained in a non-collinear magnetic structure as a result of asymmetric exchange interaction (inverse Dzyaloshinskii-Moriya (D-M) interactions).^{1,2} Later on, it was demonstrated that symmetric exchange interaction from collinear magnetic structure could also induce ferroelectricity and magnetoelectric coupling.³⁻⁵ Magnetism induced ferroelectricity due to exchange-striction was reported for orthorhombic perovskites RFeO_3 (R= rare-earth) with a collinear magnetic structure, on which spin-orbit coupling does not have significant role.^{4,6} It is now clear that exchange-striction has a dominant role on ME coupling and induced ferroelectricity for the multiferroic oxides RMn_2O_5 ^{3,7} and Ising-chain magnet $\text{Ca}_3\text{CoMnO}_6$,⁵ as well as in 1D-organic magnet⁸ showing spin-Peierls instability (dimerization due to exchange-striction). Predicted in other systems as well⁹, magnetic exchange-striction is also probably responsible for spin driven pyroelectricity in the non-collinear ferrimagnet $\text{CaBaCo}_4\text{O}_7$.^{10,11}

Among the multiferroic oxides, the one containing Co^{2+} are of peculiar interest. $\text{Ca}_3\text{CoMnO}_6$ is the first compound where exchange-striction takes place along with a peculiar

$\uparrow\uparrow\downarrow\downarrow$ collinear spin structure containing Mn^{4+} (d^3) and high spin Co^{2+} (d^7) ions, which macroscopically generates electrical polarization at the onset of magnetic ordering.⁵ This oxide shows a one dimensional Ising character of the spins, with chains of dimeric units built up of MnO_6 octahedra and CoO_6 trigonal prisms sharing faces. ME coupling and multiferroicity was also observed for the compound $\text{Lu}_2\text{CoMnO}_6$ with a ($\uparrow\uparrow\downarrow\downarrow$) spin structure arising from Co^{2+} and Mn^{4+} ions alternatingly located in corner-shared octahedral environments.^{12–16} $\text{Ca}_3\text{CoMnO}_6$ belongs to a large series of frustrated spin chain oxides $\text{A}_3\text{MM}'\text{O}_6$ ($\text{A}=\text{Ca}, \text{Sr}, \text{M}/\text{M}' = \text{transition element}$) with a triangular configuration which have been shown to exhibit exotic magnetism, based on weak inter-chain interactions compared to intra-chain interactions.^{17–24} In this family, $\text{Ca}_3\text{Co}_{2-x}\text{Mn}_x\text{O}_6$ ($x \neq 1$), $\text{Ca}_3\text{Co}_2\text{O}_6$ and $\text{Ca}_3\text{Co}_{1.4}\text{Rh}_{0.6}\text{O}_6$ also exhibit strong magnetoelectric coupling, however, ferroelectricity does not appear exactly at the onset of the magnetic transition, unlike $\text{Ca}_3\text{CoMnO}_6$.^{25–32} Therefore, it is highly warranted to investigate the magnetoelectric coupling and multiferroicity in other Ising-chain magnets containing a different arrangement of magnetic ions (Co^{2+} and Mn^{4+}).

The spin chain oxides $\text{Sr}_{4-x}\text{Ca}_x\text{CoMn}_2\text{O}_9$ ($x=0$ to 2.7) [see Ref ^{33–37}] have an hexagonal structure closely related to that of $\text{Ca}_3\text{CoMnO}_6$, but their chains consist of trimeric units of two MnO_6 octahedra sharing faces with one CoO_6 trigonal prism (see **Fig. 1**). They are typical candidates for further investigation of magnetoelectric properties in one dimensional systems. Recent detailed studies of their magnetic properties revealed single-chain magnet (SCM) and single-ion magnet (SIM) features,^{33–36} even though these magnetic behaviors are more generally observed in molecular compounds. The title compound $\text{Sr}_2\text{Ca}_2\text{CoMn}_2\text{O}_9$ ($x=2$) exhibits several similarities with $\text{Ca}_3\text{CoMnO}_6$, such as, Ising-chain magnetism containing high spin Co^{2+} and Mn^{4+} , geometrical frustration, but also differs in its magnetic ground state. Indeed, the different nature of the polyhedral units, “ Mn_2Co ” instead of “ MnCo ”, induces different intra-chain interactions. In $\text{Sr}_2\text{Ca}_2\text{CoMn}_2\text{O}_9$, it is necessary to take into account 4 exchange coupling J_i , leading to a ($\uparrow\downarrow\uparrow$) spin structure,³³ compared to $3J_i$ in $\text{Ca}_3\text{CoMnO}_6$ which shows the ($\uparrow\uparrow\downarrow\downarrow$) arrangement. Experimentally, a long-range ordered (LRO) magnetic state with a clear susceptibility peak at a Neel temperature T_N around 28 K is observed in $\text{Sr}_2\text{Ca}_2\text{CoMn}_2\text{O}_9$, compared to the restricted order observed in $\text{Ca}_3\text{CoMnO}_6$.

Therefore, the Ising-chain magnet $\text{Sr}_2\text{Ca}_2\text{CoMn}_2\text{O}_9$, exhibits many new physics features, which tempted us to investigate dielectric, magnetoelectric and possible ferroelectric behavior in this system. Considering the originality of spin dynamics in this material, we have specially focused on how dielectric constant responds for different frequencies and magnetic fields compared to that of magnetism.

II. Experimental Details

The sample was prepared by solid-state method as described in Ref.³³ The ac magnetization was performed as a function of temperature in presence of different dc magnetic fields using an ACMS option commercial **Physical Properties Measurements System** (PPMS, Quantum design). For dielectric measurements, electrodes were painted on the two opposite large facets of the sample (dense platelet of surface $(2.0 \times 3.4) \text{ mm}^2$ and thickness 0.6 mm) with silver epoxy (Dupont 4929N) cured during one day at room temperature. The measurements were then carried out by impedance analyzer (LCR meter, E4886A, Agilent Technologies) as a function of temperature and magnetic field using a home-made cryogenic insert integrated to PPMS. The data reported in this publication have been recorded in the E//H geometry. Measurements for the $\text{E} \perp \text{H}$ have given similar results. At the low temperature of measurements, the small value of the loss tangent $\tan\delta$ ($T \leq 5.10^{-2}$) confirms the highly insulating nature of this system, and allows to extract the intrinsic dielectric constant.

III. Results

Evidence of magnetoelectric coupling

The previous magnetic studies of this oxide³³ showed that in absence of dc magnetic field, the ac susceptibility $\chi'(T)$ exhibits a frequency independent peak characteristic of T_N at 28 K, followed by a frequency dependence behavior around 10 K (T_b).

The $\chi'(T)$ and $\chi''(T)$ curves (**Fig. 2a** and **Fig. 2b** respectively) recorded for a fixed frequency of 10 kHz in presence of various magnetic fields (0 – 80 kOe) confirm the previous magnetic study³⁷ and show the significant impact of an applied magnetic field on the magnetism. In absence of magnetic field, χ' exhibits a peak at T_N , followed by a broad hump around 10 K (T_b), and then sharply falls below 10 K, while χ'' exhibits a sharp peak at 8 K and a very weak peak around 28 K. Under a dc magnetic field of 10 kOe, T_N shifts to 26 K, whereas the low temperature feature T_b remains unchanged. Under a dc magnetic field of 30 kOe, a broad peak is observed around 20 K in $\chi'(T)$ followed by a change in slope around 10 K, while $\chi''(T)$ clearly exhibits both features in form of a peak \sim 20 K and \sim 10 K (see **Fig. 2a**). For a field of 50 kOe, the peak at T_N shifts further to lower temperature and nearly superimposes with the 10 K feature, as revealed by the broad bump in $\chi'(T)$. Therefore, T_N continuously shifts to lower temperature with increasing magnetic field, whereas the peak position of T_b remains nearly the same. This is consistent with antiferromagnetic inter-chain interactions and also with earlier studies of the dc magnetization.^{33,37} The absolute magnitude of ac susceptibility is usually decreased and becomes broad in presence of high dc magnetic field.

The temperature evolution of the dielectric constant $\epsilon'(T)$ (**Fig. 2c**) and dielectric loss tangent $\tan\delta(T)$ (**Fig. 2d**) of this oxide for nearly the same 10 kHz frequency and the same applied magnetic fields (H/E) shows that the dielectric and magnetic properties are closely correlated to each other. In the absence of magnetic field, ϵ' slowly increases with decreasing temperature from 50 K, and then sharply drops below \sim 10 K (T_b) down to 2 K. The loss part $\tan\delta$ is nearly constant with decreasing T and then sharply increases below \sim 10 K with a peak around 7 K. Thus, ϵ' and $\tan\delta$ trace the feature \sim T_b , mimicking the magnetism, but do not show any peak at T_N in absence of magnetic field, unlike $\chi'(T)$. Under a magnetic field of 1 kOe, no peak is detected at T_N as well (not shown here). In contrast, under a magnetic field of 5 kOe a peak is observed at the onset of magnetic ordering T_N for both real and loss part of dielectric constant. It is followed by a maximum at a temperature $T \sim T_b$. The magnitude of dielectric constant at T_N and T_b becomes stronger with increasing the magnetic field. The maximum of the dielectric constant in the higher temperature region (peak position at T_N) shifts to lower temperature with increasing H , that is, ϵ' and $\tan\delta$ show a peak below \sim 28 K for 5 kOe, which shifts to 26 K for 10 kOe, as observed in magnetism. The peak position at T_b remains nearly the same with increasing H for $H \leq 10$ kOe. Under a 30 kOe magnetic field, $\epsilon'(T)$ yields a clear broad peak around 20 K, similar to the shift of T_N and consistent with AFM ordering. The peak position related to T_N is shifted to lowest temperature with increasing further the magnetic field (say 50 kOe) and finally overlaps with the feature at T_b under a very high magnetic field (say 80 kOe). A careful analysis of $\tan\delta(T)$ reveals that two features (at T_N and T_b) can be clearly distinguished for $H \leq 50$ kOe, whereas, only one peak is observed around 7 K for $H = 80$ kOe, as observed in ac susceptibility. A clear view of temperature dependent magnetic susceptibility and dielectric constant for 10 kHz in presence of 10 kOe is shown in the **Fig. 3** to show the one-to-one correspondence between the anomalies observed in magnetism and dielectric. It demonstrates ME coupling in this compound. The magnitude of ϵ' always increases with increasing the magnetic field throughout the temperature, showing a positive ME effect. Note

that the change in ε' is almost negligible at low temperature below 25 K for low magnetic fields (see Fig. 2c for $H=0, 5, 10$ kOe), but it increases significantly at high field (see Fig. 2c for $H=30, 50, 80, 140$ kOe).

To further confirm the spin-dipole coupling and to precise the magnetic field values where the ME effect occurs, we have measured the fractional change of isothermal dielectric constant ($\Delta\varepsilon' = [\varepsilon'(H) - \varepsilon'(0)] / \varepsilon'(0)$) as a function of magnetic field at different temperatures, as shown in **Fig. 4**. A positive ME effect is observed for all the measured temperatures, including temperatures larger than $T_N \sim 28$ K. It is still significant in magnitude at $T=30, 40$ K, and tends to disappear at 70 K. Here, it is worth noting that the magnetic susceptibility measurements indicate that the Curie-Weiss regime of a pure paramagnetic state is reached only for $T \gtrsim 50$ K (see **Fig. 5**), what is consistent with the persistence of short-range magnetic correlation above T_N . Then, it can be inferred that the such coupling in this intermediate temperature range is a manifestation of magneto-elastic coupling in the presence of such short-range magnetic correlations, as observed in many other frustrated systems, including the Ising cobaltite $\text{Ca}_3\text{Co}_2\text{O}_6$.^{30,31,38,39} In the ordered state $T < T_N$, the ME effect is significantly different, and is triggered by temperature dependent magnetic field ($H \sim 20$ kOe at $T=10$ K and decreasing with the increase of temperature). The latter corresponds to the metamagnetic transition observed in dc magnetic fields, which was previously ascribed to a field-induced breaking of the partially disordered antiferromagnetic (PDA) order (due to interchain exchange coupling and Zeeman energy competition).³³ Here, it is worth noting that our sample is polycrystalline. The random orientation of grains significantly broadens this metamagnetic transition over a large field range.

Spin and dipolar dynamics in presence of dc magnetic field

To understand the spin and dipolar dynamics and the correlation between them as a result of ME coupling, we have performed frequency dependent ac susceptibility and dielectric measurements under various dc magnetic fields. The evolution of $\chi'(T)$ and $\varepsilon'(T)$ for different frequencies under a magnetic field of 10 kOe shows that the ac-susceptibility and dielectric properties exhibit a similar frequency dependence (**Fig. 6**). The huge frequency dependence behavior in ac $\chi(T)$ around 10 K (T_b) for 10 kOe (Fig.6b) is similar to that for $H=0$ (see Ref.³⁷ for ac $\chi(T)$ for dc $H=0$). The feature around T_N (~ 26 K) in presence of 10 kOe dc magnetic field exhibits a weak frequency dependence behavior (see **Fig. 6b**), unlike that for dc $H=0$. Such a frequency dependence (though very small) in presence of high dc magnetic field at T_N is not usual in the case of a perfect long-range ordered system. Formation of different magnetic domains instead of perfect 3D ordering has been previously reported at the onset of T_N $\text{Ca}_3\text{CoMnO}_6$.⁵ In $\text{Sr}_2\text{Ca}_2\text{CoMn}_2\text{O}_9$, a detailed experimental investigation has shown that a peculiar pretransitional regime, with frequency dependent susceptibility features, takes place slightly above T_N .³⁷

The maximum in $\varepsilon'(T)$ shifts to higher temperature with increasing frequency, revealing dipolar-relaxation of this system. For 10 kOe, the maximum in ε' shifts from 10 K to 15 K for the frequency of 11-120 kHz respectively (see **Fig. 6c**). It is to be noted that the maximum in χ' for 10 kHz in ac magnetic susceptibility exactly matches with the maximum in dielectric for this frequency (see **Fig. 3** for a better view). The relaxation time (τ), calculated from imaginary part of ac susceptibility and dielectric constant (i.e. $\chi''(T, f)$ and $\varepsilon''(T, f)$ (where, $\varepsilon'' = \varepsilon' \times \tan\delta$) is plotted in **Fig. 6a** as a function of $1/T$. In the high temperature limit, the variation has an Arrhenius form [$\tau = \tau_0 \exp(\Delta/T)$, where τ_0 is the pre-exponential factor, i.e. attempt time and Δ is the activation energy], It is followed by a trend to saturation at lowest temperature, in a

way consistent with SIM.³³ The fitting in the Arrhenius limit gives $\tau_0=3*10^{-9}$ sec and $\Delta= 47$ K. The fact that the relaxation times of magnetic and dielectric susceptibilities obey to the same law clearly indicates that both the spin and dipolar relaxation should arise from same origin/mechanism.

The spin-chain compounds Ca_3CoBO_6 , (B= Co, Mn, Rh) also exhibit frequency dependence spin-relaxation and dipolar-relaxation behavior at low T below PDA, and it was a categorized as “multi-glass-like” behavior,^{30–32} similar to “magnetoelectric multiglass” where dipolar relaxation arises due to spin-dipole coupling in a spin-glass system^{40–43} In $\text{Sr}_2\text{Ca}_2\text{Mn}_2\text{CoO}_9$, we have previously shown³³ that the spin relaxation takes origin in a SIM mechanism with thermally driven spins blocking. Then, considering that spin and dipolar relaxation obey the same mechanism, we name this phenomenon a “multiblocking”effect.

Finally, we have tried to measure the electrical polarization via pyroelectric measurements, cooling the sample from 40K down to 5K using different voltage poling (corresponding to a maximum electric field of 285 kV/m), with and without applied magnetic field. We were unable to detect a significant pyroelectric current and an electrical polarization. At this point it should be noted that the polycrystalline nature of the sample can strongly affect its polar response. The statistical averaging of the local polarization in grains decreases the macroscopic polarization and the electrical coercivity can increase due to domain walls pinning at grain boundaries and defects. These two extrinsic effects can impede an efficient poling. Another possibility arises from the genuine nature of the polar order in this sample, which is dominated by dynamical effects as discussed above. In ferroelectrics with time dependent dielectric properties (relaxor-like), a characteristic slim hysteresis loop is observed with a very small remnant polarization. It seems reasonable to anticipate similar characteristics in our sample, and a very small polarization can be inferred. Hence, we termed the title compound as magnetoelectric instead of magnetodielectric throughout the manuscript.

IV. Discussion

Let us compare our results with $\text{Ca}_3\text{CoMnO}_6$, GdCrTiO_5 and $\text{Lu}_2\text{CoMnO}_6$, and discuss the similarities and contrasts. First it has to be noted that no magnetic susceptibility peak and no sharp anomaly of the dielectric constant are observed at the reported magnetic transition in $\text{Ca}_3\text{CoMnO}_6$.⁵ Later, the observation of electrical polarization at temperatures far above PDA ordering for $\text{Ca}_3\text{Co}_{2-x}\text{Mn}_x\text{O}_6$ solid solutions makes this system more intriguing.²⁷ For our compound, we observe both a clear magnetic susceptibility peak at zero magnetic field and a magnetic field induced dielectric peak for $H \geq 5$ kOe. Similar magnetic field induced dielectric peak (and a ferroelectric transition) above 10 kOe was reported for GdCrTiO_5 , which is derived from the well-known multiferroic RMn_2O_5 structure.^{39,44} $\text{Lu}_2\text{CoMnO}_6$ exhibits a clear peak in dielectric constant around magnetic ordering in absence of magnetic field which is suppressed with increasing magnetic field, unlike our title compound.

The frequency dependent behavior at low temperature below PDA ($T < T_N$) clearly yields a one-to-one correspondence between spin and dipoles for this compound. Such a consistency between the frequency dependence of magnetic susceptibility and dielectric constant was noted in $\text{Ca}_3\text{Co}_2\text{O}_6$,³⁰ and clues of similar behavior can be observed in $\text{Ca}_3\text{CoMnO}_6$,⁵ and $\text{Ca}_3\text{Co}_{1.3}\text{Mn}_{0.7}\text{O}_6$.²⁷ This strongly suggests that such a characteristic is a common feature in this type of Ising type spin-chain system, though the nature of magnetism is different for different compound.

Now, we will discuss the possible mechanism of creating dipoles. Exchange-striction driven ferroelectricity was first discussed in $\text{Ca}_3\text{CoMnO}_6$,⁵ where competing nearest-neighbor

ferromagnetic and next-nearest-neighbor antiferromagnetic exchange interactions were proposed. The associated $\uparrow\uparrow\downarrow$ magnetic ordering is responsible for electrical polarization which arises from uncompensated elemental dipoles between cations of different charges (Co^{2+} and Mn^{4+}).⁵ Later, it was found from DFT calculations that all exchange interactions are antiferromagnetic,⁴⁵ but can be still compatible with the $\uparrow\uparrow\downarrow$ magnetic structure and exchange striction mechanism.

Let us now address the possible origin of ME coupling in $\text{Sr}_2\text{Ca}_2\text{CoMn}_2\text{O}_9$. The spins order $\uparrow\downarrow\uparrow$ ($\text{Co}^{2+} - \text{Mn}^{4+} - \text{Mn}^{4+}$) results from a compromise between four exchange couplings J_1, J_2, J_3, J_4 (see Ref.33), compared to the 3 dominant exchange couplings in $\text{Ca}_3\text{CoMnO}_6$. In the supplemental material, we investigate and conclude on the possibility of an exchange-striction mechanism similar to that proposed for $\text{Ca}_3\text{CoMnO}_6$. In particular, provided that J_2 and J_4 are not strictly equal to each other, a bonus in exchange energy can be gained by introducing a slight move between two consecutive $\uparrow\downarrow\uparrow$ units (trimerization process). The mechanism is summarized in **fig.7**. Note that, in principle, a sharp dielectric peak should occur at the zero field T_N , whereas it is observed only for $H \geq 5$ kOe. It indicates that either the displacement of the atom is not sufficient to achieve an appreciable dielectric polarization value (measurable within the resolution of the instrument) below 5 kOe only, or the ME coupling mechanism needs a certain magnetic field to be effective. Due to the compensation of the + and - chains (Fig.8), the dielectric response should arise from the incoherent chains only, which possibly need a large enough magnetic field to be significantly polarized.

Fig.8 shows the spin states of $\text{Sr}_2\text{Ca}_2\text{CoMn}_2\text{O}_9$ for $T < T_N$ under different magnetic fields. **Fig. 8a** represents the PDA state in the zero field limit. **Fig. 8b** illustrates the “moderate field” regime ($0 < H < 2T$). The T_N is still marked by a peak in magnetic χ and dielectric susceptibility ϵ' and its temperature shifts to lower values as H is increased as classically observed for an AF transition (fig.2). Note that only the incoherent chains are progressively polarized by the magnetic field, which induces unbalance between the up and down $\uparrow\downarrow\uparrow$ units, and increases both χ and ϵ' . Note that because of the polycrystalline nature of our sample, the metamagnetic transition and the associated dielectric features are spread over a broad field range. The high field regime, where all spins are magnetically polarized and where T_N is no more depicted, i.e. far above the metamagnetic transition, is shown in **fig. 8c**. The absence of PDA feature in magnetism in presence of very high magnetic field (say, $H > 50$ kOe) and thus the absence of dielectric peak agrees with this exchange-striction mechanism of ME coupling. This field driven sequence from PDA/metamagnetic/polarized states can be directly seen on the $\Delta\epsilon'(H)$ curves at 20 K and 15K of the **fig. 4** and is responsible for the S shape and shows consistently the saturation of the ME effect at large field. At the lowest temperatures, the blocking effect takes place even at large field and interestingly, impedes the saturation of the ME effect.

V. Conclusion

In summary, we have investigated the magnetoelectric properties of the Ising chain-magnet $\text{Sr}_2\text{Ca}_2\text{CoMn}_2\text{O}_9$ through frequency dependence ac susceptibility and dielectric constant in presence of different magnetic fields as a function of temperature. A direct coupling between spin dynamics and dipole dynamics is evidenced by the same time scales measured in the dipolar relaxation and spin-relaxation below PDA, which is attributed to “multiblocking” effect. This is proposed as a common characteristic of strongly anisotropic, Ising-like, spin-chain series, despite different magnetic ground states. We discuss and argue on an exchange-striction origin of the magnetoelectric coupling in this exciting compound.

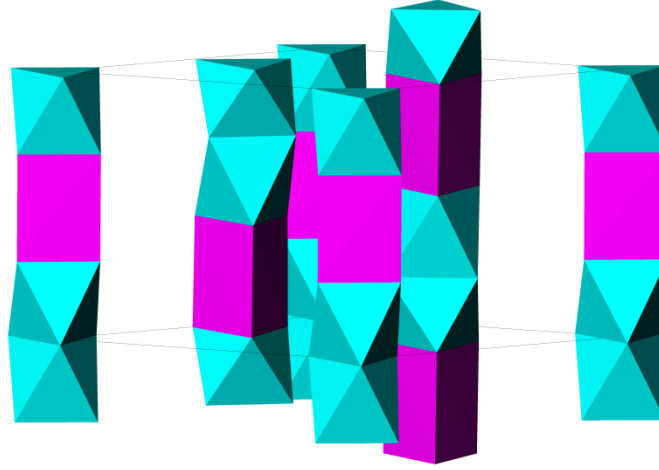


Figure 1: Schematic structure of the stoichiometric spin chains oxide $\text{Sr}_2\text{Ca}_2\text{Mn}_2\text{CoO}_9$. The chains distributed on a triangular network are built up of face sharing CoO_6 trigonal prisms (magenta) and MnO_6 octahedra (cyan). Sr and Ca distributed between chains are omitted for the sake of clarity.

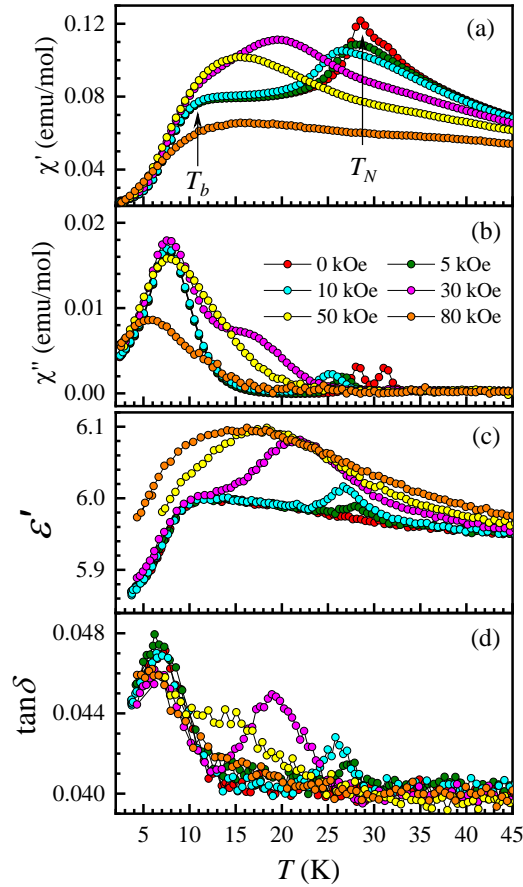


Figure 2: Real (a) and imaginary (b) part of ac susceptibility as a function of temperature for various fields from 0 to 80 kOe and a fixed frequency of 10 kHz. (c) and (d) are the real part and loss tangent of dielectric constant, for the same fields and for a fixed frequency of 11.1 kHz for the compound $\text{Sr}_2\text{Ca}_2\text{Mn}_2\text{CoO}_9$, respectively.

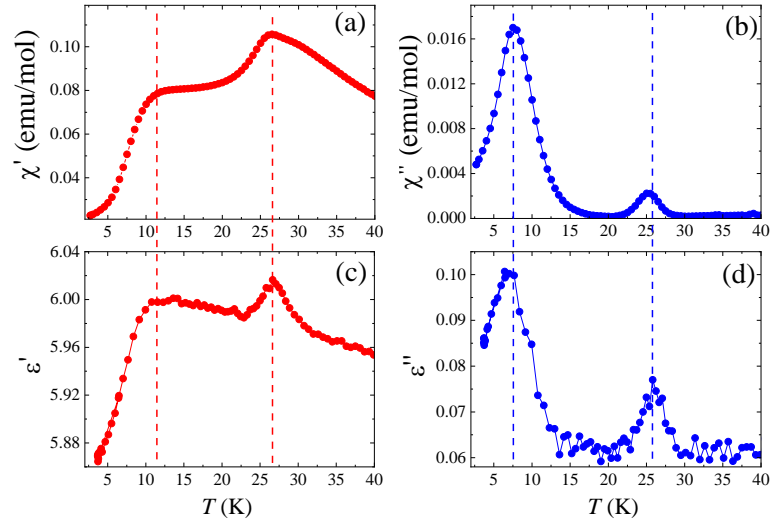


Figure 3: In-phase (a) and out-of-phase (b) magnetic susceptibility recorded in 1T at a frequency of 10 kHz. In-phase (c) and out-of-phase (b) dielectric constant recorded in the same magnetic field and at a very close frequency (11.1 kHz). The dashed lines show the correspondences between the magnetic and dielectric data.

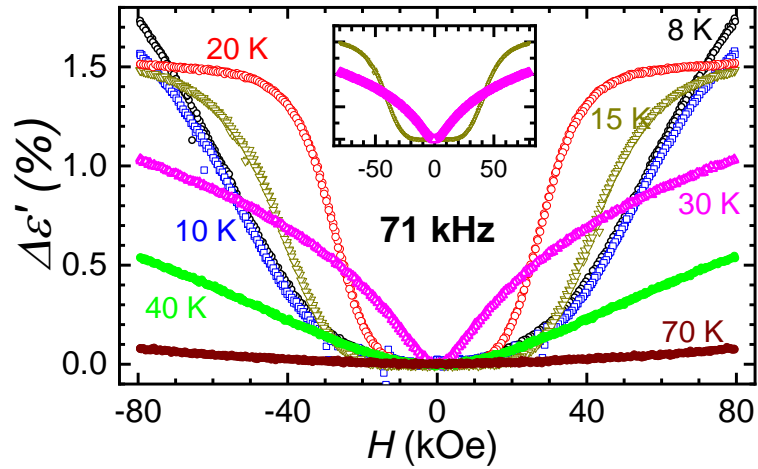


Figure 4: Fractional change of dielectric constant as a function of magnetic field for selective temperatures and a fixed frequency of 71 kHz. The inset is an enlargement of $\Delta\varepsilon'$ vs. H at 15 K and 30 K in order to highlight the change of shape.

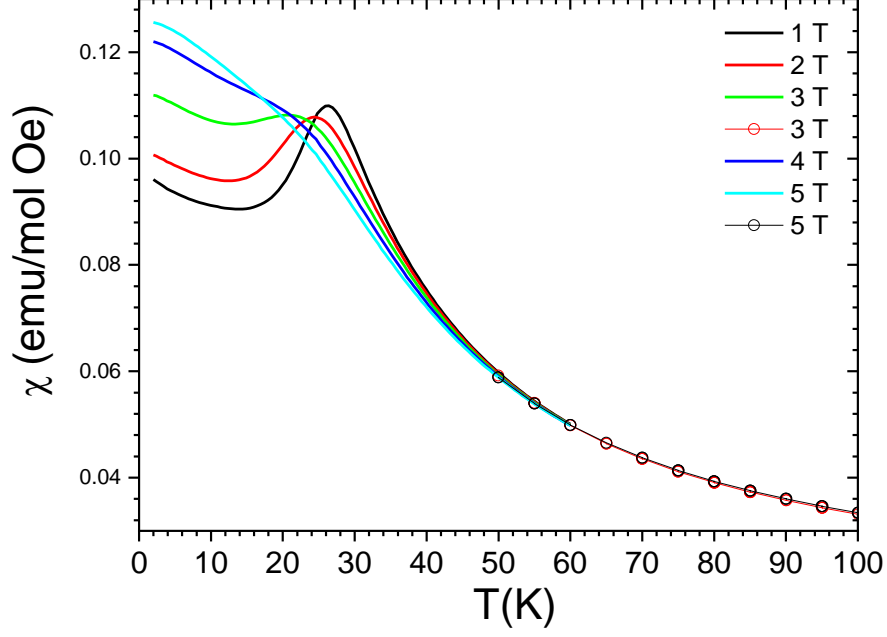


Figure 5 : Susceptibility curves recorded in Field Cooled Cooling (FCC) modes. A genuine paramagnetic behavior is recovered only at $T \sim 50\text{-}60$ K, i.e significantly above the Neel temperature.

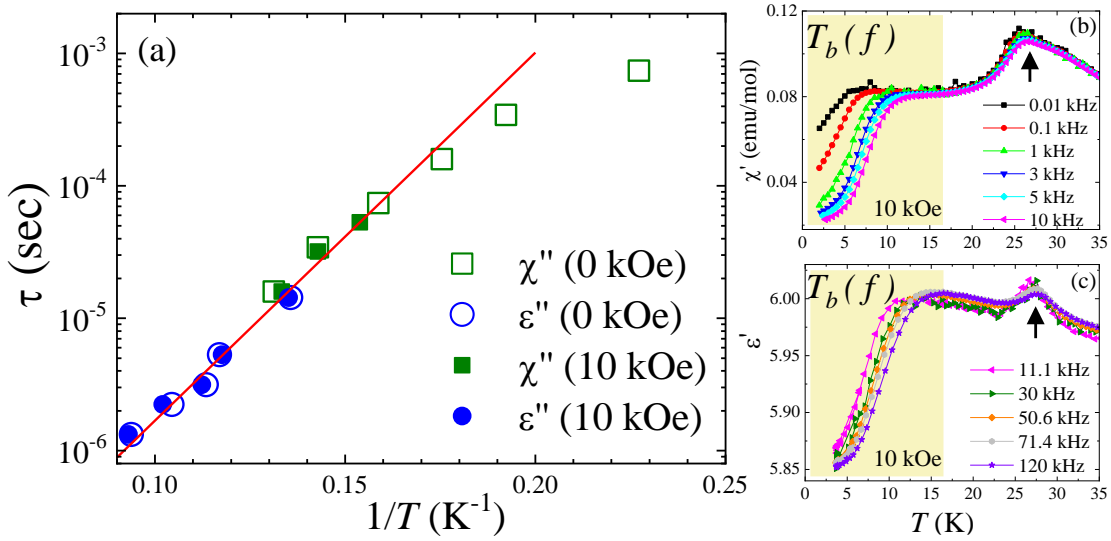


Figure 6: The panel (a) reports the relaxation times derived from the maxima of $\chi''(T, f)$ and $\varepsilon''(T, f)$ in both zero-field and 1 T. The red line is a fitting of the high-T part of these data to an Arrhenius law [$\tau = \tau_0 \exp(\Delta/T)$] leading to $\Delta \sim 47$ K and $\tau_0 \sim 3 \cdot 10^{-9}$ sec. The panels (b) and (c) display the in-phase magnetic susceptibility and dielectric constant measured in 1 T at various frequencies. The yellow boxes highlight the T -range over which the blocking effect takes place (starting below a frequency-dependent blocking temperature T_b). The peak at higher temperature marks the T_N whose position is virtually frequency-independent.

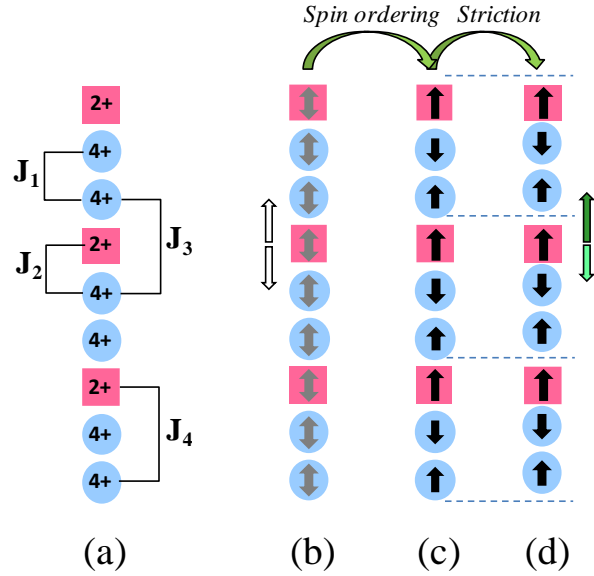


Figure 7: Schematic representation of the alternation of Co^{2+} and Mn^{4+} along the chains. Panel (a) highlights the four types of coupling that must be taken into account. Panel (b) corresponds to the paramagnetic state; the spins are not ordered and the electric dipole between Co^{2+} and Mn^{4+} cancel each other out (white arrows). (c) Spin ordering taking place for two thirds of the chains below T_N . (d) Exchange striction accompanying the spin ordering (see text), which induces unbalance between the electric dipoles around each Co^{2+} (green arrows). This yields the appearance of a net polarization along the chain.

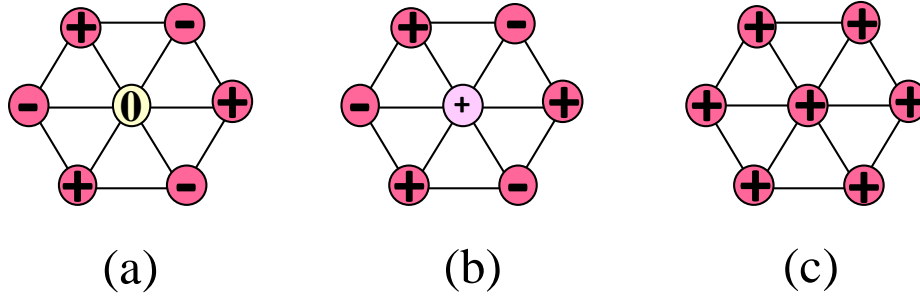


Fig. 8: Top views of the triangular chain lattice, for various regimes of applied field, at $T < T_N$. The symbols + and - correspond to chain obeying $\uparrow\downarrow\uparrow$ ordering (as shown in Fig. 6c) with the Co^{2+} spin oriented up or down respectively. The symbols 0 refer to the incoherent chains of the PDA order, having a zero net magnetization. (a) PDA state in zero-field; (b) Moderate magnetic fields ($0 < H < 2$ T) tend to polarize the incoherent chains without affecting the antiferromagnetic coupling between + and - chains; (c) High fields ($H > 2$ T) can break the antiferromagnetic interchain coupling, leading to full polarization of all the chains.

Acknowledgement:

We would like to thank Laurence Hervé (CRISMAT) for her work on the sample synthesis, and the ANR ([ANR-16-CE08-0023](#)) for the financial support.

References:

- ¹ Y. Tokura, S. Seki, and N. Nagaosa, *Rep. Prog. Phys.* **77**, 076501 (2014).
- ² T. Kimura, T. Goto, H. Shintani, K. Ishizaka, T. Arima, and Y. Tokura, *Nature* **426**, 55 (2003).
- ³ L.C. Chapon, P.G. Radaelli, G.R. Blake, S. Park, and S.-W. Cheong, *Phys. Rev. Lett.* **96**, 097601 (2006).
- ⁴ I.A. Sergienko, C. Şen, and E. Dagotto, *Phys. Rev. Lett.* **97**, 227204 (2006).
- ⁵ Y.J. Choi, H.T. Yi, S. Lee, Q. Huang, V. Kiryukhin, and S.-W. Cheong, *Phys. Rev. Lett.* **100**, 047601 (2008).
- ⁶ Y. Tokunaga, S. Iguchi, T. Arima, and Y. Tokura, *Phys. Rev. Lett.* **101**, 097205 (2008).
- ⁷ G. Yahia, F. Damay, S. Chattopadhyay, V. Balédent, W. Peng, E. Elkaim, M. Whitaker, M. Greenblatt, M.-B. Lepetit, and P. Foury-Leylekian, *Physical Review B* **95**, (2017).
- ⁸ F. Kagawa, S. Horiuchi, M. Tokunaga, J. Fujioka, and Y. Tokura, *Nature Physics* **6**, 169 (2010).
- ⁹ M. Pregelj, O. Zaharko, A. Zorko, Z. Kutnjak, P. Jeglič, P.J. Brown, M. Jagodič, Z. Jagličić, H. Berger, and D. Arčon, *Phys. Rev. Lett.* **103**, 147202 (2009).
- ¹⁰ K. Singh, V. Caignaert, L.C. Chapon, V. Pralong, B. Raveau, and A. Maignan, *Phys. Rev. B* **86**, 024410 (2012).
- ¹¹ V. Caignaert, A. Maignan, K. Singh, Ch. Simon, V. Pralong, B. Raveau, J.F. Mitchell, H. Zheng, A. Huq, and L.C. Chapon, *Phys. Rev. B* **88**, 174403 (2013).
- ¹² N. Lee, H.Y. Choi, Y.J. Jo, M.S. Seo, S.Y. Park, and Y.J. Choi, *Appl. Phys. Lett.* **104**, 112907 (2014).
- ¹³ S. Chikara, J. Singleton, J. Bowlan, D.A. Yarotski, N. Lee, H.Y. Choi, Y.J. Choi, and V.S. Zapf, *Phys. Rev. B* **93**, 180405 (2016).
- ¹⁴ J. Blasco, J. García, G. Subías, J. Stankiewicz, J.A. Rodríguez-Velamazán, C. Ritter, J.L. García-Muñoz, and F. Fauth, *Phys. Rev. B* **93**, 214401 (2016).
- ¹⁵ S. Yáñez-Vilar, E.D. Mun, V.S. Zapf, B.G. Ueland, J.S. Gardner, J.D. Thompson, J. Singleton, M. Sánchez-Andújar, J. Mira, N. Biskup, M.A. Señarís-Rodríguez, and C.D. Batista, *Phys. Rev. B* **84**, 134427 (2011).
- ¹⁶ V.S. Zapf, B.G. Ueland, M. Laver, M. Lonsky, M. Pohlit, J. Müller, T. Lancaster, J.S. Möller, S.J. Blundell, J. Singleton, J. Mira, S. Yáñez-Vilar, and M.A. Señarís-Rodríguez, *Phys. Rev. B* **93**, 134431 (2016).
- ¹⁷ H. Kageyama, K. Yoshimura, K. Kosuge, H. Mitamura, and T. Goto, *J. Phys. Soc. Jpn.* **66**, 1607 (1997).
- ¹⁸ V. Hardy, S. Lambert, M.R. Lees, and D. McK. Paul, *Phys. Rev. B* **68**, 014424 (2003).
- ¹⁹ E.V. Sampathkumaran, N. Fujiwara, S. Rayaprol, P.K. Madhu, and Y. Uwatoko, *Phys. Rev. B* **70**, 014437 (2004).
- ²⁰ V. Hardy, D. Flahaut, M.R. Lees, and O.A. Petrenko, *Phys. Rev. B* **70**, 214439 (2004).
- ²¹ S. Agrestini, L.C. Chapon, A. Daoud-Aladine, J. Schefer, A. Gukasov, C. Mazzoli, M.R. Lees, and O.A. Petrenko, *Phys. Rev. Lett.* **101**, 097207 (2008).
- ²² E.V. Sampathkumaran and A. Niazi, *Phys. Rev. B* **65**, 180401 (2002).
- ²³ S. Rayaprol, K. Sengupta, and E.V. Sampathkumaran, *Solid State Communications* **128**, 79 (2003).
- ²⁴ O.A. Petrenko, J. Wooldridge, M.R. Lees, P. Manuel, and V. Hardy, *Eur. Phys. J. B* **47**, 79 (2005).
- ²⁵ P. Ding, L. Li, Y.J. Guo, Q.Y. He, X.S. Gao, and J.-M. Liu, *Appl. Phys. Lett.* **97**, 032901 (2010).
- ²⁶ L. Lin, Y.J. Guo, Y.L. Xie, S. Dong, Z.B. Yan, and J.-M. Liu, *Journal of Applied Physics* **111**, 07D901 (2012).
- ²⁷ J. Shi, J.D. Song, J.C. Wu, X. Rao, H.L. Che, Z.Y. Zhao, H.D. Zhou, J. Ma, R.R. Zhang, L. Zhang, X.G. Liu, X. Zhao, and X.F. Sun, *Phys. Rev. B* **96**, 064112 (2017).

- ²⁸ N. Bellido, C. Simon, and A. Maignan, *Phys. Rev. B* **77**, 054430 (2008).
- ²⁹ P.L. Li, X.Y. Yao, K.F. Wang, C.L. Lu, F. Gao, and J.-M. Liu, *Journal of Applied Physics* **104**, 054111 (2008).
- ³⁰ T. Basu, K.K. Iyer, K. Singh, and E.V. Sampathkumaran, *Scientific Reports* **3**, 3104 (2013).
- ³¹ T. Basu, K.K. Iyer, P.L. Paulose, and E.V. Sampathkumaran, *Journal of Alloys and Compounds* **675**, 364 (2016).
- ³² T. Basu, K.K. Iyer, K. Singh, K. Mukherjee, P.L. Paulose, and E.V. Sampathkumaran, *Appl. Phys. Lett.* **105**, 102912 (2014).
- ³³ Md.M. Seikh, V. Caignaert, O. Perez, B. Raveau, and V. Hardy, *Phys. Rev. B* **95**, 174417 (2017).
- ³⁴ K. Boulahya, M. Parras, J.M. González-Calbet, and J.L. Martínez, *Chemistry of Materials* **15**, 3537 (2003).
- ³⁵ K. Boulahya, M. Hernando, M. Parras, and J.M. González-Calbet, *J. Mater. Chem.* **17**, 1620 (2007).
- ³⁶ M.M. Seikh, V. Caignaert, O. Perez, B. Raveau, and V. Hardy, *J. Mater. Chem. C* **6**, 3362 (2018).
- ³⁷ V. Hardy, V. Caignaert, O. Pérez, L. Hervé, N. Sakly, B. Raveau, Md.M. Seikh, and F. Damay, *Phys. Rev. B* **98**, 144414 (2018).
- ³⁸ T. Basu, V.V.R. Kishore, S. Gohil, K. Singh, N. Mohapatra, S. Bhattacharjee, B. Gonde, N.P. Lalla, P. Mahadevan, S. Ghosh, and E.V. Sampathkumaran, *Scientific Reports* **4**, 5636 (2014).
- ³⁹ T. Basu, D.T. Adroja, F. Kolb, H.-A. Krug von Nidda, A. Ruff, M. Hemmida, A.D. Hillier, M. Telling, E.V. Sampathkumaran, A. Loidl, and S. Krohns, *Phys. Rev. B* **96**, 184431 (2017).
- ⁴⁰ V.V. Shvartsman, S. Bedanta, P. Borisov, W. Kleemann, A. Tkach, and P.M. Vilarinho, *Phys. Rev. Lett.* **101**, 165704 (2008).
- ⁴¹ D. Choudhury, P. Mandal, R. Mathieu, A. Hazarika, S. Rajan, A. Sundaresan, U.V. Waghmare, R. Knut, O. Karis, P. Nordblad, and D.D. Sarma, *Phys. Rev. Lett.* **108**, 127201 (2012).
- ⁴² K. Singh, A. Maignan, C. Simon, V. Hardy, E. Pachoud, and C. Martin, *J. Phys.: Condens. Matter* **23**, 126005 (2011).
- ⁴³ S. Sharma, T. Basu, A. Shahee, K. Singh, N.P. Lalla, and E.V. Sampathkumaran, *Phys. Rev. B* **90**, 144426 (2014).
- ⁴⁴ T. Basu, K. Singh, S. Gohil, S. Ghosh, and E.V. Sampathkumaran, *Journal of Applied Physics* **118**, 234103 (2015).
- ⁴⁵ Y. Zhang, H.J. Xiang, and M.-H. Whangbo, *Phys. Rev. B* **79**, 054432 (2009).

Supplemental Material

ARGUMENTS FOR AN EXCHANGE STRICTION MECCGANISM AS THE ORIGIN OF SPIN-DIPOLE COUPLING IN $Sr_2Ca_2CoMn_2O_9$

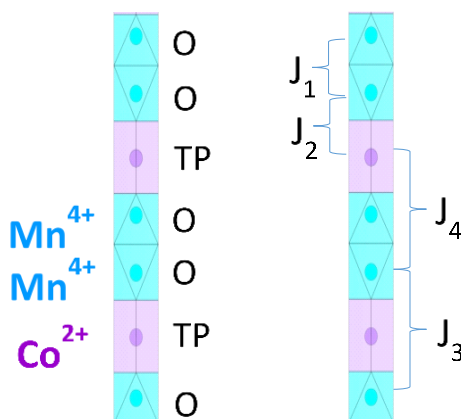


Fig. A1 : Side views of the type of spin chains present in $Sr_2Ca_2CoMn_2O_9$. Left panel emphasizes their structure, that is made of a regular stacking of face-sharing octahedra (noted O, in cyan) hosting Mn^{4+} , and of trigonal prisms (noted TP, in magenta) hosting Co^{2+} . Right panel indicates the four types of exchange interactions involved in the derivation of the intrachain spin configuration. They corresponds to first or second neighbours, which can also be referred to as nearest-neighbours (nn) or next-nearest-neighbours (nnn), respectively.

Fig A1 displays the structure of the spin chains of $Sr_2Ca_2CoMn_2O_9$, specifying the nature of the polyhedra and of the cations (left), as well as the nature of the first and second neighbours interactions (right).

The third-neighbours interactions within the chains can be considered to be significantly weaker, as attested to by the value of the Co^{2+} - Co^{2+} coupling (~ 1 K) determined in the isostructural $Ba_4CoPt_2O_9$ (where Pt^{4+} is nonmagnetic) [N. Sakly, V. Caignaert, O. Perez, L. Herve, B. Raveau, V. Hardy. *J. Magn. Magn. Mater.* 508, 166877 (2020)]. Previous works on related compounds showed that the coupling J_1 , J_2 , and J_3 are all antiferromagnetic (AF). Quantitative estimates of the interactions (J_1, J_2, J_3) can be derived from studies on $Sr_4Mn_2NiO_9$ and Ca_3CoMnO_6 [A. El Abed, E. Gaudin, J. Darriet, and M.-H. Whangbo, *J. Solid State Chem.* 163, 513 (2002); Y. Zhang, H. J. Xiang, and M.-H. Whangbo, *Phys. Rev. B* 79, 054432 (2009)]. Adopting the convention « $2k_B J_i S_j S_{j+1}$ » for the exchange energies (with $S = 3/2$ for

both Co^{2+} and Mn^{4+}) one obtains $J_1 \sim 35$ K, $J_2 \sim 26$ K, and $J_3 \sim 27$ K. No estimate of J_4 is available, but this coupling can be expected to be AF (like J_1, J_2, J_3) and of the same order of magnitude.

One is thus facing a situation of geometrical frustration along the chains. In practice, a certain spin configuration should be favored by the competition between the four couplings. Finding this most favorable compromise in terms of interaction energy is the purpose of the following analysis.

First of all, let us recall that, owing to the strong Ising character of the Co^{2+} in TP (transmitted to the Mn^{4+} via the magnetic interactions), one can consider only two possible states for each spin, i.e., either \uparrow or \downarrow along the easy axis (i.e., oriented along the chain direction). Second, since the most favorable spin configuration is driven by the competition between nn and nnn interactions, its determination requires to consider two *nuclear repeat units*. Let us choose Mn-Co-Mn as this basic nuclear unit ; the portion of spin chain used for the calculation of the exchange energy is materialized by the yellow box in Fig. A2 (for practical convenience, the spins direction is drawn perpendicularly to the chain, but this does not affect the calculations).

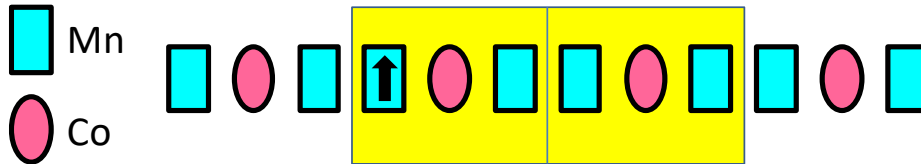


Fig. A2 : Schematic picture of the chain structure, made of a regular stacking between Mn^{4+} (in octahedra) and Co^{2+} (in trigonal prisms). The « spin repeat unit » is highlighted by the yellow box which contains two « nuclear repeat units ». The spin of the first site is arbitrarily chosen to be *up* (\uparrow).

With six adjacent spin sites, there are in principle 64 possible configurations, but one can fix the orientation of one of the spins (\uparrow) without loss of generality ; this reduces the number of configurations to 32. Then, since the interactions are predominantly AF, the configurations of spins with (6 \uparrow) or (5 \uparrow & 1 \downarrow) are very unlikely. So, we will limit ourselves to the configurations (4 \uparrow & 2 \downarrow) and (3 \uparrow & 3 \downarrow). Eliminating the equivalent configurations (via horizontal or vertical mirrors) one is left with only 15 different spin configurations. Making use of the estimates of (J_1, J_2, J_3), the exchange energies associated to each of them is plotted versus J_4 in Fig. A3.

One observes that the groundstate can correspond to four different spin configurations, depending on the J_4 value. An enlargement of Fig. A3 limited to these potential groundstates is shown on Fig. A4, along with the nature of these four spin states. When considering the most likely values of J_4 (AF interaction of amplitude close to the other nnn interaction, i.e. J_3), it remains two possible configurations which are characterized by the same exchange energy independent of J_4 . These configurations labelled ① and ③ are shown in Fig. A4.

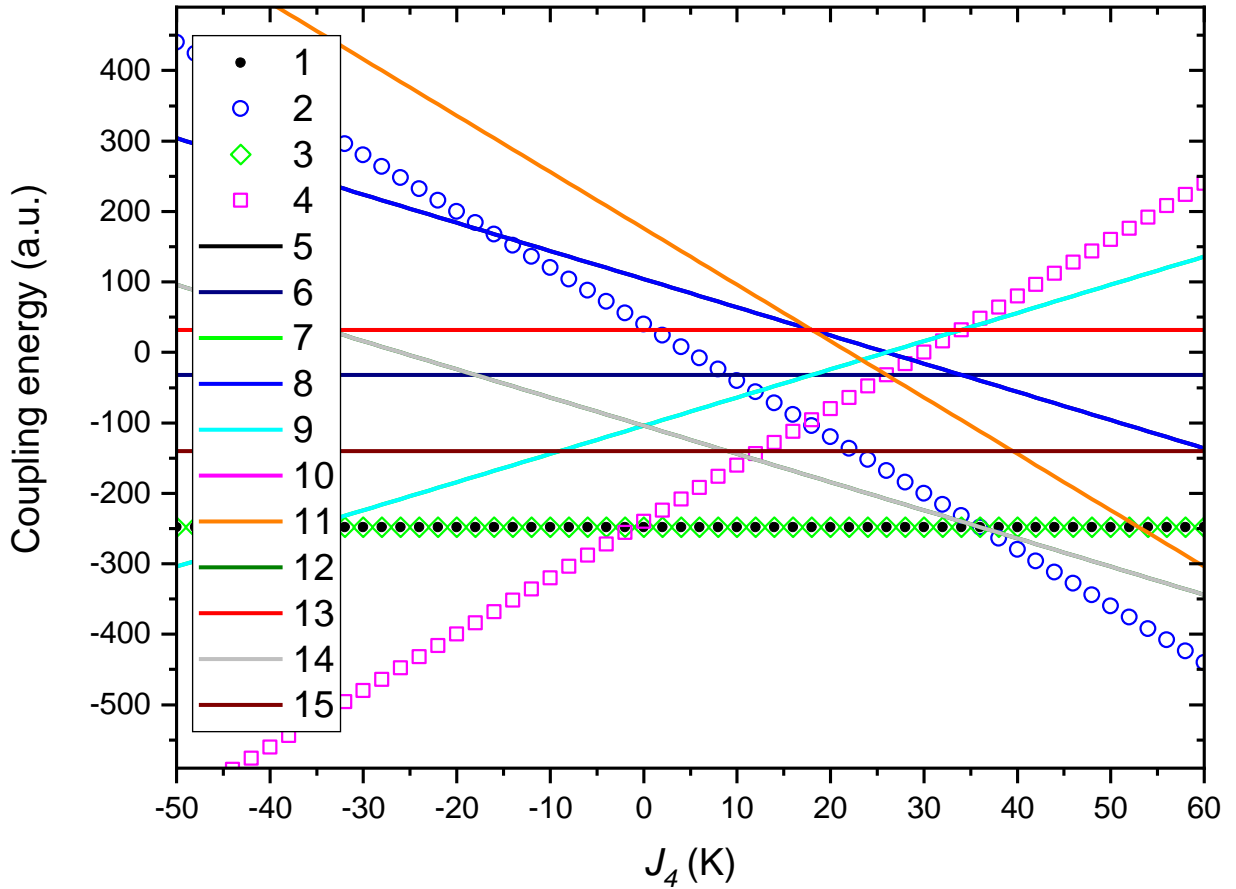


Fig A3 : Exchange energy associated to the spin repeat unit of Fig A2, calculated for the 15 possible spin configurations, as a function of the unknown parameter J_4 . For (J_1, J_2, J_3) , we used the estimates derived from parent compounds (see text).

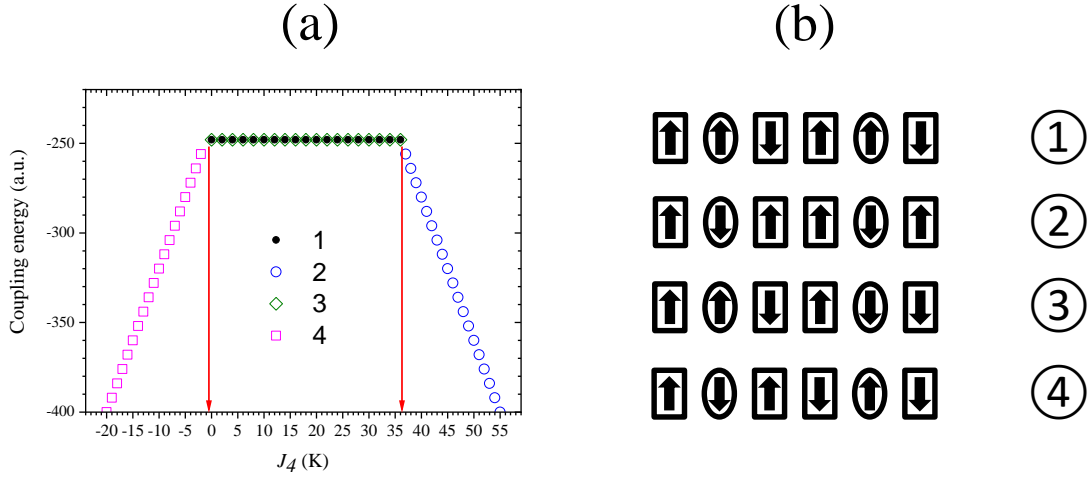


Fig A4 : (a) Enlargement of Fig. A3 focusing on the four configurations susceptible to be the groundstate. These spin configurations are displayed in panel (b) (ellipses are Co²⁺ and rectangles are Mn⁴⁺).

The spin configuration ① actually corresponds to the ($\uparrow\downarrow\uparrow$) order previously reported in paper [1] (referring to a Co-Mn-Mn unit). It has a net magnetization associated to the Co²⁺ spins. The spin configuration ③ corresponds to an AF order ; Such a magnetic structure should be characterized by a doubling of parameter (not found experimentally in neutron diffraction experiments) and it should have a zero net magnetization (at odds with the experimental magnetization data). Accordingly, the only spin configuration that is consistent with the present analysis and the experimental data is the configuration ①. Even though ① and ③ are degenerate in zero field (and when limiting the interactions up to second neighbours), it can be noted that ① is favored by application of magnetic field, owing to the Zeeman energy term.

Exchange-striction phenomenon

Let us now address the origin of a magnetoelectric response in Sr₂Ca₂Mn₂CoO₉. In what follows, we investigate the possibility of a mechanism similar to that described in the parent compound Ca₃CoMnO₆, where electrical polarization originates from uncompensated elemental dipoles between cations of different charges (Co²⁺ and Mn⁴⁺). The underlying mechanism is basically a magnetostriction phenomenon in which the spin system can lower its exchange energy by moving the positions between some of the cations along the chains.

Looking at the spin configuration ①, one observes that both the interactions J_1 and J_3 are fully satisfied, while it is not the case for J_2 and J_4 . Thereafter, we limit ourselves to the mechanisms susceptible to induce electrical dipoles, i.e. various bond lengths between Co²⁺

and Mn^{4+} . We also make use of the reasonable assumption that the coupling intensity between any pair of spins increases as the interdistance between them is decreased. Starting from the spin configuration ①, it turns out that the exchange energy can be further optimized (i.e. decreased) by moving apart the spin at the tick positions shown in Fig. A5, either at the upper ones (full lines) to gain energy via J_2 or at the lower ones (dashed lines) to gain energy via J_4 . To be more quantitative, let us adopt the following assumptions : (i) The overall chain length is kept constant and the Co positions are fixed ; (ii) There is an overall shift of the Mn_2 pair; one Mn moves away from one neighboring Co ,whereas the second Mn becomes closer to the second neighboring Co ; (iii) Accordingly, J_1 and J_3 are not modified, while J_2 splits into $(J_2 - dJ_2)$ and $(J_2 + dJ_2)$, as well as J_4 into $(J_4 - dJ_4)$ and $(J_4 + dJ_4)$; (iv) All the J_i and the dJ_i are positive.

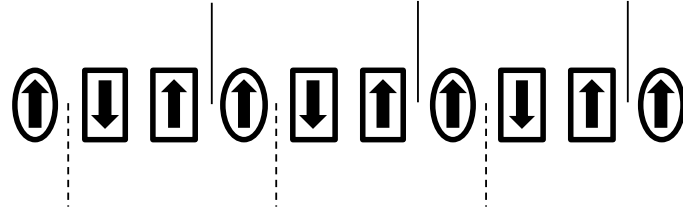


Fig. A5 : Groundstate spin configuration ① with Co^{2+} in ellipses and Mn^{4+} in rectangles The ticks mark the positions for which extra spacings can be beneficial in terms of exchange energy.

Calculations of the exchange energies are then carried out as done previously. With increased intercationic separation at the upper ticks, the exchange energy turns to $E_{ex} = E_{\textcircled{1}} - 8(dJ_2 - dJ_4)$. Such a distortion is thus authorized if $dJ_2 > dJ_4$, leading to the modified spin structure (a) in Fig. A6. For spacings at the lower ticks, $E_{ex} = E_{\textcircled{1}} - 8(dJ_4 - dJ_2)$, making such a distortion favorable for $dJ_4 > dJ_2$. This induces the structure (b) in Fig . A6 which also corresponds to (b') (equivalent via a vertical mirror).

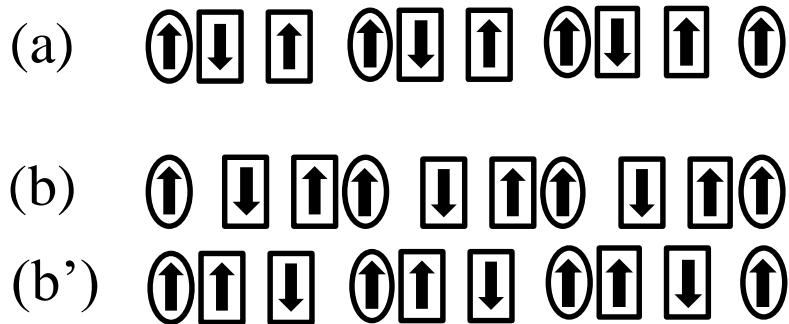


Fig. A6 : Schematic pictures of the spin chain structures resulting from exchange-striction effects applied to the groundstate configuration ① (see text).

In both cases, one observes the same kind of trimerization involving Co-Mn-Mn units. In practice, one can thus reasonably expect that a exchange-striction mechanism [either (a) or (b)] can take place in $\text{Sr}_2\text{Ca}_2\text{Mn}_2\text{CoO}_9$ provided that J_2 is not strictly equal to J_4 . AT this stage, it must be specified that we have only dealt with the exchange energy in the above analysis. In principle, the onset of magnetostriction also requires that the *gain in magnetic energy exceeds the cost in elastic energy* (associated to the distortion of the chain structure). This second energy term is not taken into account in the present approach.